LANGMUIR

pubs.acs.org/Langmuir Article

Nonclassical Surface Nucleation of 6CB at the Air−Liquid Interface of a 6CB Oil-in-Water Nanoemulsion

Jin Tae Park, Govind Paneru, Masao Iwamatsu, Bruce M. Law,* and Hyuk Kyu Pak*

Cite This: *Langmuir* 2021, 37, 9588−9596 Read Online

ACCESS | Metrics & More | Article Recommendations | Supporting Information

ABSTRACT: The surface tension of a freshly extruded pendant drop of a nanoemulsion, 4-cyano-4′-hexylbiphenyl or 6CB (a liquid crystal) in water, exhibits an unusual surface nucleation phenomenon. Initially the surface tension is that of pure water; however, after a surface nucleation time, the surface tension decreases suddenly in magnitude. This nucleation time, of hundreds to thousands of seconds, depends strongly upon (i) the 6CB concentration in water, (ii) the 6CB nanodroplet size, and (iii) the temperature. Similar behavior is observed in both the isotropic and nematic phases of 6CB; thus, this surface nucleation phenomenon is unrelated to this system's liquid crystalline properties. The observed surface nucleation behavior can be explained via considerations of the nanoemulsion's bulk entropy together with the number of 6CB nanodroplets in the vicinity of the surface.

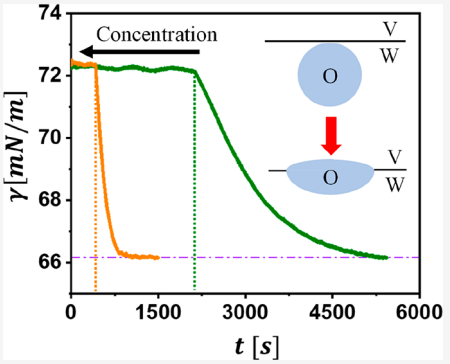

1. INTRODUCTION

Nucleation at surfaces, and within confined systems, has been the subject of extensive study in the past. Wetting layer nucleation at the noncritical surface of a critical binary liquid mixture was quantified many years ago.[1,2] Herminghaus et al.[3] quantified the spinodal dewetting of unstable films initiated by the heterogeneous or homogeneous nucleation of holes in that film while, very recently, Campbell and Christenson[4] observed the nucleation of crystals from a saturated vapor phase in confined pores.

In this publication, we report the experimental observation of a new type of surface nucleation behavior found at the air−liquid surface of a nanodroplet emulsion. The nanodroplet emulsion that was selected in these initial experiments is perhaps more complex than one would have desired as it consists of nanodroplets of a liquid crystal in water. Nevertheless, we demonstrate that the experimental properties that are observed can be successfully explained by simply considering generic binary liquid mixture properties of the nanoemulsion without having to explicitly account for any liquid crystalline characteristics. We expect that this surface nucleation behavior is a generic property of nanodroplet emulsions and hence that it should be very common in nature. Figure 1 schematically illustrates the generic surface nucleation process that is expected to be present in nanodroplet emulsions. The emulsion consists of nanodroplets of oil, dispersed in water (Figure 1a). A proportion of the oil droplets, N_s/N_b, are in the vicinity of the air−water interface where N_s (N_b) is the number near the surface (in the bulk phase). At the beginning of the experiment, the oil droplets in the vicinity of the surface are entirely encompassed within the

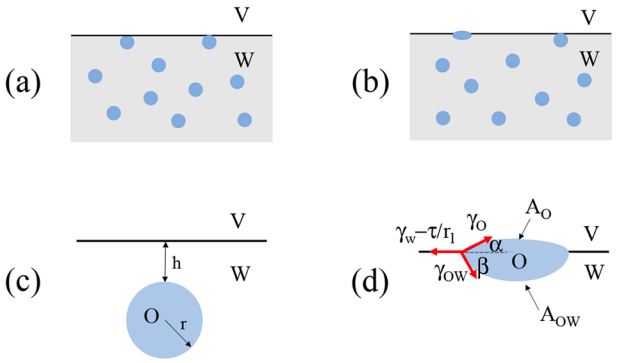

Figure 1. (a) Initial air−water surface in contact with a nanodroplet emulsion (blue circles = nano-oil droplets). (b) A nanosurface droplet has undergone a nonclassical surface nucleation event (blue oval shape at air−water surface). (c) Enlargement of part a depicting an initial surface oil droplet at the air−water surface a distance h from the air−water surface. (d) Enlargement of a nano-oil droplet in mechanical equilibrium at the air−water surface where the contact angles α and β obey the Neumann−Young equations (eqs 1a and 1b), and γ_i and A_i are, respectively, the surface tension and area of interface i, while τ is the line tension, and r_l is the lateral radius of the oil droplet.

Received: June 3, 2021
Revised: July 15, 2021
Published: July 30, 2021

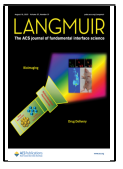

https://doi.org/10.1021/acs.langmuir.1c01487
Langmuir 2021, 37, 9588−9596

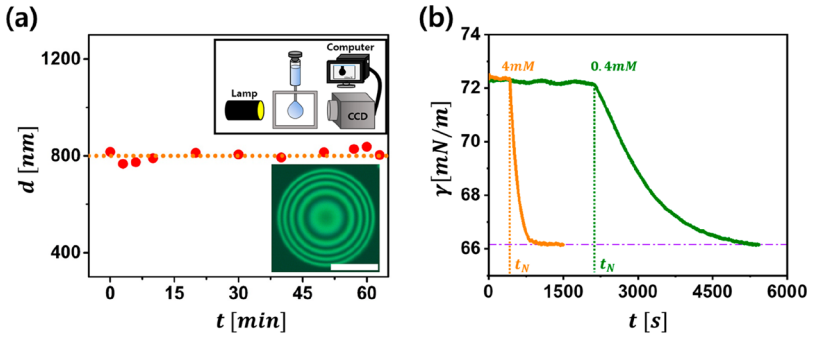

Figure 2. (a) Mean 6CB droplet diameter d in water (4 mM) as a function of solution aging. Insets: pendant drop tensiometer setup used in the surface tension measurements (upper); microscopic interferogram of a 6CB droplet at an air−dispersion surface, scale bar = 30 μm (lower). (b) Liquid/vapor surface tension γ variation with time t for an emulsion of 6CB droplets in a water droplet at two different 6CB concentrations for 6CB nanodroplet diameter d = 800 nm.

water phase; thus, their effective contact angle with the air−water surface is 180° (Figure 1c). However, as $\gamma_o < \gamma_w$, where γ_o (γ_w) is the air−oil (air−water) surface tension, this surface droplet will make a finite contact angle lens at this interface when in mechanical equilibrium, as schematically depicted in Figure 1d. The contact angle $\alpha + \beta$ for this lens (where angles α and β are defined in Figure 1d) will depend upon γ_w, γ_o, as well as the magnitude of the oil−water interfacial tension γ_{ow} and the line tension τ at the three-phase oil−water−air contact line. For sufficiently small droplets, so that gravitational effects can be ignored, the surface tensions, line tension, and contact angles must obey the Neumann−Young equations with[5]

$$\gamma_o \cos\alpha + \gamma_{ow} \cos\beta = \gamma_w - \frac{\tau}{r_l} \tag{1a}$$

$$\gamma_o \sin\alpha = \gamma_{ow} \sin\beta \tag{1b}$$

where r_l is the lateral radius of the droplet. In transforming from Figure 1c to Figure 1d, the volume of the oil droplet is conserved. The transformation from Figure 1a to Figure 1b illustrates the "nonclassical" surface nucleation event described in this publication where a single surface nanodroplet transforms from a spherical droplet, within the water phase, to a surface lens at the air−water interface. It takes time, the surface nucleation time t_N, for a nanodroplet to undergo this transformation. The purpose of this publication is (i) to experimentally quantify t_N which is found to depend upon the bulk concentration x of oil in the water phase, the 6CB nanodroplet diameter d, as well as the temperature T; and (ii) to provide a theoretical explanation for these experimental observations.

This publication is organized as follows. Section 2 describes the experimental technique, methods, materials, and results for the surface nucleation of oil nanodroplets at the air−water surface of a nanoemulsion. In section 3, the interplay between surface interactions and wetting phenomena is described as a prelude to a discussion of surface nucleation. Section 4 outlines a theory for nonclassical surface nucleation and compares this theory with the experimental results. The paper concludes with a summary and discussion of the experimental and theoretical results (Section 5).

2. EXPERIMENTAL METHODS AND RESULTS

Sample Preparation. Initially, a simplified preparation method (Method A) was used to prepare 6CB droplets, of diameter d ~800 nm, in an aqueous solution. Later, it was realized that a more meticulous preparation method (Method B) was required in order to prepare droplets of differing diameters in an aqueous solution.

Method A. The 4-cyano-4′-hexylbiphenyl, 6CB, (>98%) was purchased from Tokyo Chemical Industry and used as received. At room temperature, 6CB is in the nematic liquid crystalline phase and is partially soluble in water (solubility in water[6] 3.2 × 10^{-5} g/L). Nanoemulsions of differing 6CB concentrations in water are prepared using the following procedure. A 4 mM 6CB dispersion in water, for example, is prepared by mixing 10.6 μL of 6CB in 10 mL of deionized water. This solution is shaken vigorously for 30 s followed by sonication at 40 kHz at maximum power in a Branson Company Model 3800 sonication bath for 30 min. This step is repeated 4 times. The solution is milky due to the formation of a nanoemulsion of 6CB droplets in water. The mean diameter d of 6CB droplets in water, as confirmed by dynamic light scattering (Figure 2a), is found to be ~800 nm and independent of time.

Method B. Changes in the sonication power and sonication bath height allow one to control the 6CB dispersion droplet size (Table 1).

Table 1. Sonication Power, Bath Height, and 6CB Droplet Diameter

sonication power P at f = 40 kHz (W)	H (mm):V (L)	diameter d (nm)
90−100	20:0.93	1632 ± 258
120−130	40:1.86	1184 ± 158
120−130	30:1.395	832 ± 107
120−130	20:0.93	641 ± 76
150−160	40:1.86	525 ± 101
150−160	20:0.93	403 ± 96

In order to prepare a particular dispersion droplet size, the 6CB + water solution was shaken vigorously for 20 s followed by sonication at a power P and height H (Table 1) at 40 kHz for 10 min using a Powersonic 605 instrument from Hwashin Technology Company. This step was repeated 6 times. (The Powersonic 605 instrument possesses an internal bath length and width of 300 and 155 mm, respectively. The sonication bath volume V is changed by varying the liquid bath height H.) Droplet dispersions, for all 6CB droplet sizes studied, were found to be stable as a function of time. 6CB droplets in water are expected to be negatively charged[7] which probably plays a role in the droplet dispersion stability.

Surface Tension Measurements. Dynamic surface tension measurements $\gamma(t)$ of a 6CB dispersion in water (Figure 2b), at various bulk 6CB concentrations, were measured in a chamber at a temperature either below (22.0 ± 0.1 °C, room temperature) or above (32.0 ± 0.1 °C) the isotropic/nematic transition via the pendant drop technique.[8] The chamber humidity was kept high (~55%) throughout the experiment to minimize water evaporation; droplet volume changes were less than 1%/h at room temperature. For 6CB, the isotropic/nematic transition temperature T_{IN} = 28.3

https://doi.org/10.1021/acs.langmuir.1c01487
Langmuir 2021, 37, 9588−9596

°C.[9] Figure 2a (upper inset) schematically depicts the tensiometer setup (Ramé-Hart Instrument Co., Model 250 with DROPimage Advanced software).

Microscopic Reflection Interferometry. Interferograms at wavelength λ = 530 nm (Figure 2a, lower inset) of small ∼25 μL 6CB droplets deposited onto the air−liquid surface of a 10 mM 6CB dispersion in water enabled the internal droplet contact angle $\alpha + \beta = 0.22° \pm 0.04°$ to be measured. Interferograms were measured 1−2 h after the initial 6CB droplet deposition in order to allow for any liquid disturbances to dissipate.

Experimental Results. Figure 2b depicts the time variation of the liquid−vapor surface tension γ for a dilute emulsion of 6CB droplets of diameter d ∼800 nm dispersed in a water droplet at two different 6CB concentrations, 0.4 and 4 mM. These surface tension measurements were obtained using the pendant droplet technique where, at time t = 0 s, a pendant droplet of volume V_p ∼14 μL consisting of a 6CB dispersion in water, prepared using Method A, was dispensed from a syringe and suspended in air from a stainless steel needle. An analysis of the shape of the suspended droplet allows one to determine the surface tension variation with time shown in Figure 2b. At t = 0, the droplet exhibits a surface tension close to that for pure water where, after a surface nucleation time t_N, the surface tension abruptly starts to decrease with time. The surface tension eventually reaches its equilibrium value $\gamma \approx 66.15$ mN/m, which is independent of the 6CB concentration, after a decay time t_D. Figure 2b demonstrates that although the initial and final surface tensions are independent of the concentration x of 6CB in water, both t_N and t_D depend sensitively upon this 6CB concentration. In the following, all 6CB concentrations have been converted to volume fractions determined from

$$\phi = V_{6CB}/(V_{6CB} + V_w) \approx 10^{-3} MW_{6CB} x/\rho_{6CB} = 2.613 \times 10^{-4} x \quad (2)$$

where V_i is the volume of component i, x is the 6CB concentration in mM, and the molecular weight and density of 6CB are, respectively, MW_{6CB} = 263.377 g/mol and $\rho_{6CB} = 1.008 \times 10^3$ kg/m^3. Within this pendant droplet of volume V_p, the number of 6CB droplets in this nanodispersion is given by

$$N = 6\phi V_p/\pi d^3 \quad (3)$$

The quantities N, ϕ, and d all play an important role in the surface nucleation process, as described below.

The variation of t_N with 6CB volume fraction ϕ is shown in Figure 3 (blue open circles for $d \simeq$ 800 nm). Similar nucleation times are found both above (red open circles, Figure 3) and below (blue open circles) T_{IN}; therefore, the variation of t_N with ϕ is the result of general bulk and surface properties of 6CB, relative to water, rather than specifically due to the liquid crystalline nature of 6CB. Figure 3 also depicts a rather similar behavior for t_N as a function of ϕ for differing 6CB droplet diameters of $d \simeq$ 400 nm (orange squares) and $d \simeq$ 1200 nm (green triangles). In the following, the $d \simeq$ 800 nm data, which is the most well characterized, will be primarily discussed. The other 6CB droplet diameters ($d \simeq$ 400 and 1200 nm) will be discussed later.

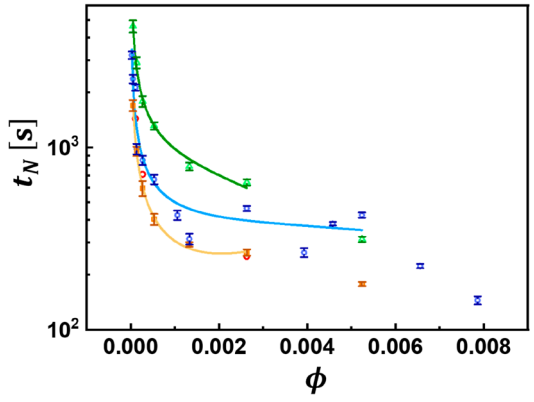

Figure 3. Variation of surface nucleation time t_N with 6CB volume fraction ϕ and 6CB droplet size d: $d \approx$ 400 nm (orange squares), 800 nm (blue circles), and 1200 nm (green triangles) at T = 22 °C (where $T < T_{IN}$) and $d \approx$ 800 nm (red circles) at T = 32 °C (where $T > T_{IN}$). The solid lines are best fits to eq 26 as described in the text.

3. WETTING TRANSITIONS AND SURFACE INTERACTIONS

Wetting phenomena and surface interactions are discussed in this section so that the reader more fully understands the conditions under which surface nucleation is occurring in Figure 3. Short- and long-ranged surface interactions play an important role in determining the type of wetting (partial, pseudopartial, or complete wetting) that can occur at a liquid−vapor surface and, as a consequence, whether a wetting transition is first or second order and, correspondingly, whether or not surface nucleation is possible.[10−13] For our system, the relevant surface tensions (γ_w, γ_{6CB}, and γ_{6CB-w}), refractive indices (n), and static dielectric constants ($\varepsilon(0)$) are listed in Table 2 at a temperature of 25 °C. The spreading coefficient is defined as[12]

$$S = \gamma_w - (\gamma_{6CB} + \gamma_{6CB-w}) \quad (4)$$

Table 2. Surface Tension, Refractive Index, and Dielectric Constant at 25 °C

	γ (mN/m)	n	$\varepsilon(0)$
water	71.97[17]	1.3325[17]	77.936[17]
6CB	32.8,[9] 33.94[a]	∼1.6[18]	9.5[19]
6CB−water	16.2[a]		

[a]Our measurements.

In the partial wetting region, $S < 0$, and a droplet would possess a finite, nonzero contact angle θ at a liquid−vapor surface. The data in Table 2 indicate that $S > 0$ for our system; consequently, the short-ranged surface tension forces dictate that the air−water surface will be covered by a 6CB layer, of thickness l, when in mechanical and thermodynamic equilibrium. This layer thickness is also influenced by the long-ranged van der Waals surface energy, which varies as W/l^2 in the nonretarded regime. If the Hamaker constant $W < 0$ ($W > 0$), then the van der Waals interaction thins (thickens) this surface layer, and the system is in the pseudopartial (complete) wetting regime. In the pseudopartial wetting regime, a droplet at the surface will be in coexistence with this mesoscopic surface film, whereas in the complete wetting regime, the contact angle of any surface droplet is zero, and the surface film thickness is divergent ($l \to \infty$). The Hamaker constant

$$W \approx W_{\nu=0} + W_{\nu>0} \quad (5)$$

is to a good approximation the sum of a zero frequency $W_{\nu=0}$ and an optical frequency $W_{\nu>0}$ contribution. $W_{\nu=0} \propto \varepsilon(0)_w - \varepsilon(0)_{6CB}$ ($W_{\nu>0} \propto n_w^2 - n_{6CB}^2$) depends upon the dielectric constant (refractive index squared) difference,[14] which determines the sign of this contribution. (A comment on notation: the Hamaker constant used by Israelachvili,[14] A, is related to our definition of the Hamaker constant via $W = -A/12\pi$; hence, A and W are of opposite signs.) According to Table 2, $W_{\nu=0} > 0$ ($W_{\nu>0} < 0$) tends to thicken (thin) the 6CB

https://doi.org/10.1021/acs.langmuir.1c01487
Langmuir 2021, 37, 9588−9596

film. In most situations, $W_{\nu>0}$ is the dominant contribution and normally determines the sign of W. From section 13.5 in Israelachvili[14] and the data in Table 2, assuming a UV absorption frequency $\nu_e = 3 \times 10^{15}$ s^{-1} and temperature T = 300 K, the Hamaker constant for a 6CB film at the air−water surface is $W = -1.0 \times 10^{-21}$ J. In other words, our system is in the pseudopartial wetting regime with $S > 0$ and $W < 0$; this determination is consistent with our experimental observations that at late times a 6CB droplet placed at the air−dispersion interface possesses a finite contact angle with internal contact angle $\alpha + \beta = 0.22°$ (Figure 2a, lower inset) while the surface tension measurements indicate that such an air−dispersion interface will be covered with a 6CB film of surface tension 66.1 mN/m (Figure 2b).

The wetting of the air−water surface, by an oil (*n*-pentane or *n*-hexane), has been extensively studied in the past. For a droplet of pentane deposited at the air−water surface, a second-order wetting transition was observed at a wetting temperature T_{w2},[15] whereas for a hexane oil droplet, both a first-order and second-order wetting transition were observed at wetting temperatures T_{w1} and T_{w2}, respectively, where the values for T_{w1} and T_{w2} could be controlled via the addition of NaCl to the aqueous phase.[16] T_{w1} arises from a change in sign of S where below (above) T_{w1} the system is in the partial (pseudopartial) wetting regime. T_{w2} arises from a change in sign of W (for S positive) where above T_{w2} the system is in the complete wetting regime. This particular *n*-alkane/water system is rather unusual because $n(\text{oil}) \simeq n(\text{water})$, and a change in sign of $W_{\nu>0}$ can be induced via a change in temperature which correspondingly leads to a change in sign of W with temperature. For our 6CB−water system, the refractive index difference $\Delta n = n(\text{oil}) - n(\text{water})$ is a factor of 10 larger than for the alkane−water system; hence, our 6CB−water system will not be near any thermally induced second-order wetting transition. Second-order wetting transitions are continuous surface phase transitions where l increases continuously upon approaching T_{w2}. Accompanying this continuous change in l will be a continuous change in the surface tension of the oil-coated air−water surface. First-order wetting transitions possess a very different physical character in comparison with second-order wetting transitions. Below (above) T_{w1}, at equilibrium, the surface is covered with an adsorption layer (wetting layer of thickness l). Hence, at T_{w1} (when in equilibrium), there is an abrupt change from a nanoscopic adsorption layer to a mesoscopic wetting layer of thickness l. This discontinuous change in the layer thickness is accompanied by a change in the slope of the surface tension. At temperatures *above* T_{w1}, it is possible to trap the surface in the metastable adsorption state. For a surface trapped in a metastable adsorption state to reach its equilibrium wetting state, the system must overcome a surface nucleation barrier associated with the formation of the wetting phase. It takes time, the nucleation time t_N, to surmount this surface nucleation barrier. The abrupt change in the behavior of the surface tension at nucleation time t_N, exhibited in Figure 2b, is indicative of a first-order wetting transition with the creation of a new wetting phase.

A complication for the air−water and oil−water surfaces is that hydroxyl ions (OH^-) preferentially adsorb at both of these surfaces, and hence, these surfaces are known to be negatively charged.[7] The wetting transitions T_{w1} and T_{w2}, observed for an *n*-hexane droplet deposited at the air−water surface, were consequently a sensitive function of the concentration of NaCl in the aqueous phase[16] due to these surface charging effects. The ramifications of surface charging on surface nucleation phenomena are discussed later in this publication.

4. THEORY OF NONCLASSICAL SURFACE NUCLEATION IN NANOEMULSIONS

We start by discussing surface nucleation in the absence of any surface charging; surface charging will be introduced at the appropriate place. Our most well-studied sample is for $d \simeq 800$ nm (Figure 3, blue circles); thus, we start by discussing this sample first. The surface nucleation time t_N decreases by a factor of ∼25 as the bulk 6CB volume fraction ϕ changes from 3×10^{-5} to 8×10^{-3} (x = 0.1−30 mM) . This dependence of the surface nucleation time upon bulk dispersion volume fraction has never been reported in the past, as far as the authors are aware. In this section, we attempt to ascertain the principal factors that lead to the behavior observed in Figure 3.

To place these experiments in context, we first briefly review traditional *classical* surface nucleation. In classical surface nucleation, the initial surface state, of free energy G_s^i, is metastable and possesses a higher free energy than the equilibrium surface state, of free energy G_s^f. These two free energy states are separated by a free energy barrier of height $\Delta G_s = G_s^m - G_s^i$ where G_s^m is a free energy maximum which separates G_s^i from G_s^f. It takes time for the system to "tunnel" through this free energy barrier to reach the final equilibrium state. The surface nucleation time, in this situation, is given by

$$t_N = t_o P_s^{-1} \tag{6}$$

where the probability for surface nucleation

$$P_s \propto \exp(-\Delta G_s / k_B T) \tag{7}$$

$t_o = 1/f_o$, f_o is the nucleation attempt frequency, and $k_B T$ is the thermal energy. In homogeneous classical surface nucleation ΔG_s is related to the energy involved for random thermal fluctuations to create a surface nucleus greater than a critical size V_c. Fluctuations with volume $V > V_c$ grow, whereas fluctuations with $V < V_c$ shrink. A form for ΔG_s is given in earlier work.[1] ΔG_s consists of various surface energy terms and does not exhibit a coupling to the bulk volume fraction ϕ. For classical nucleation to be the explanation for the surface nucleation phenomena observed in this publication, 6CB molecules *in the aqueous phase* would need to cluster together in the vicinity of the air−water surface and form a surface nucleus greater than the critical size. In such a situation, at fixed ϕ, the nucleation time t_N should not depend upon the 6CB droplet size d. As t_N does depend upon d (at fixed ϕ) in Figure 3 classical surface nucleation is not believed to be the explanation for the phenomenon observed herein.

For a nanoemulsion, surface nucleation is expected to occur via a radically different mechanism compared with classical surface nucleation, which we have therefore called *nonclassical* surface nucleation. In a nanoemulsion, the initial metastable state (Figure 1c) has energy

$$G_s^i = 4\pi r^2 \gamma_{ow} + A_x \gamma_w \tag{8}$$

where r is the radius of a typical emulsion droplet while $A_x = \pi r_1^2$ is the cross-sectional area of the lens at the air−water surface (Figure 1d). The final state schematically depicted in Figure 1d, which initiates the sudden decrease in the surface tension γ at time t_N, has energy

https://doi.org/10.1021/acs.langmuir.1c01487
Langmuir 2021, 37, 9588−9596

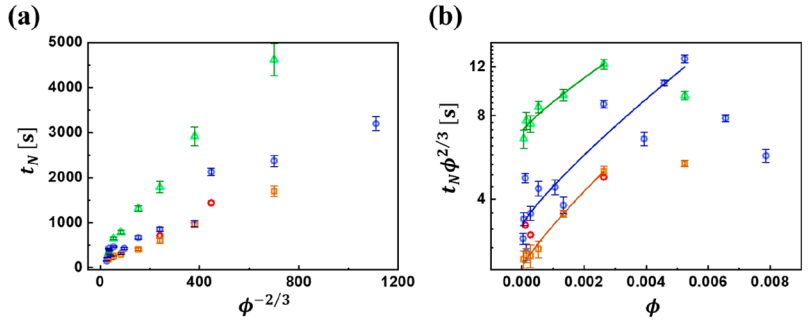

Figure 4. (a) Plot of nucleation time t_N versus $\phi^{-2/3}$ for the data in Figure 3 using the same color coding: $d \approx 400$ nm (orange squares), 800 nm (blue circles), and 1200 nm (green triangles) at $T = 22$ °C and $d \approx 800$ nm (red circles) at $T = 32$ °C. (b) Plot of $t_N\phi^{2/3}$ versus ϕ on a semilog scale where the solid line is a best fit to eq 26 as described in the text.

$$G_s^f = A_o\gamma_o + A_{ow}\gamma_{ow} + \tau 2\pi r_1 \tag{9}$$

where A_o (A_{ow}) is the area of the air−oil (oil−water) surface of the lens depicted in Figure 1d. The volume of the nanodroplet is conserved in going from Figure 1c to Figure 1d where, to ensure a thermodynamic driving force for surface nucleation, $G_s^i > G_s^f$. The evolution of a nanoemulsion drop from Figure 1c to Figure 1d is a complicated hydrodynamic process driven by an attractive van der Waals force between the oil nanodroplet and the air−water surface and a repulsive double layer force due to the negative charge on the air−water and oil−water surfaces where this surface charging is screened by counterions in solution. This physical situation is analogous to the DLVO theory[14] for the coalescence of two charged oil droplets in water except that, in the current situation, we are considering the coalescence of a charged oil droplet with the charged air−water surface. In analogy to eqs 6 and 7, for the current scenario, the nonclassical surface nucleation time is given by

$$t_N = \frac{1}{f_o}\exp\left[\frac{\Delta G_s^{nc}}{k_B T}\right] \tag{10}$$

where ΔG_s^{nc} is the nonclassical free energy barrier separating the surface states depicted in Figure 1c,d. ΔG_s^{nc} is expected to be independent of 6CB volume fraction ϕ as ΔG_s^{nc} is related to a single 6CB sphere undergoing this transition. Thus, the ϕ dependence of t_N, observed in Figure 3, can only enter via f_o. The nucleation attempt frequency f_o will be proportional to the number N_s of 6CB nanodroplets in the vicinity of the surface where N_s will depend upon bulk 6CB volume fraction. In the following, we provide an estimate for N_s. The total number of 6CB droplets in the pendant droplet

$$N \propto R^3 \tag{11}$$

where R is the radius of the pendant droplet (i.e., N is proportional to the volume of the pendant droplet). The number of 6CB droplets in the vicinity of the surface will be proportional to the area of the pendant droplet, namely

$$N_s \propto R^2 \tag{12}$$

and, therefore from eqs 11 and 12

$$N_s \propto N^{2/3} \propto \phi^{2/3} \tag{13}$$

as N is proportional to ϕ (eq 3).

Thus, this simple analysis suggests that (at constant temperature)

$$t_N = B\phi^{-2/3} \tag{14}$$

where B is expected to be a constant independent of bulk 6CB volume fraction.

Figure 4a demonstrates that t_N is, to a reasonable approximation, a linear function of $\phi^{-2/3}$ for the three differing values of d. In Figure 4b, $t_N\phi^{2/3}$ is plotted as a function of ϕ where the weak dependence upon concentration, in this figure, indicates that some element is missing from eq 14. For example, for $d \simeq 800$ nm (Figure 4, blue circles), eq 14 largely accounts for the factor of ~25 change in t_N exhibited in Figure 4a where $B_1 \simeq (6 \pm 3)$ s from Figure 4b.

In reality, eq 10 is an approximation that assumes that the change in the bulk Gibbs free energy ΔG_b is zero. In fact it is impossible to separate out the surface free energy from the bulk free energy because, in the nucleation process, the surface is populated from a droplet that originates in the bulk (or near surface). The change in the total free energy is therefore

$$\Delta G_{tot} = \Delta G_s^{nc} + \Delta G_b \tag{15}$$

and a more appropriate equation, in comparison with eq 10, is

$$t_N = \frac{1}{f_o}\exp\left[\frac{\Delta G_s^{nc} + \Delta G_b}{k_B T}\right] \tag{16}$$

The bulk free energy G_b is an extensive quantity, which depends upon the number of 6CB droplets N ($\equiv N_b$) in the bulk phase. Normally, for a semi-infinite bulk phase in contact with the surface, a single surface nucleation event would have a negligible influence on the bulk free energy G_b because N, in this case, would be very large. In the current experiments, the bulk phase (pendant droplet) is finite, rather than semi-infinite, where in addition the 6CB concentration is small. Hence, a single surface nucleation event will have a measurable influence on N and therefore on G_b. The change in the bulk Gibbs free energy ΔG_b consists of an interfacial free energy term ΔG_I, an entropy term $-T\Delta S$, and a chemical potential term $\mu\Delta N$, specifically

$$\Delta G_b = \Delta G_I - T\Delta S + \mu\Delta N \tag{17}$$

The interfacial free energy term is equal to the change in interfacial energy between Figure 1a and Figure 1b; this term is not expected to depend upon ϕ because only a single 6CB nanodrop has undergone a change in interfacial energy. Note that eq 17 neglects interactions between charged 6CB nanodroplets in the bulk aqueous phase; hence, this equation is equivalent to an ideal gas assumption (in the bulk) which will be valid at low ϕ but may fail at higher ϕ.

https://doi.org/10.1021/acs.langmuir.1c01487
Langmuir 2021, 37, 9588−9596

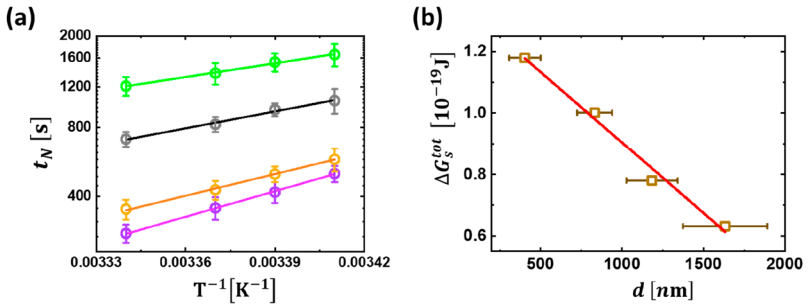

Figure 5. (a) Plot of nucleation time t_N versus $1/T$ on a semilog plot at fixed ϕ = 0.000 53 and various 6CB droplet diameters d ~403 nm (purple), 832 nm (brown), 1184 nm (black), and 1632 nm (green) . (b) Plot of ΔG_s^{tot} versus d determined from the slope of the lines in Figure 5a. The red line is a linear fit to eq 25 as described in the text.

The entropy term depends upon the number of different ways that the oil phase can be arranged within the system. In the case of a colloidal oil dispersion in water, the configurational entropy can be derived from a statistical analysis of the number of oil droplets:[20]

$$S = -\frac{Nk_B}{\phi}[\phi \ln \phi + (1-\phi)\ln(1-\phi)] \tag{18}$$

where N is the number of oil droplets in the colloidal dispersion, and ϕ is the volume fraction of the dispersed oil phase in water. The number of arrangements accessible to the oil phase in an emulsified state is greater than in a nonemulsified state; however, if an emulsified state is thermodynamically unstable, then the system always prefers the formation of separated phases.[21] The entropy change between the final and initial states is therefore

$$\Delta S = S_f - S_i = \frac{N\varepsilon k_B}{\phi}[\phi \ln \phi + (1-\phi)\ln(1-\phi)] \tag{19}$$

where ε is the fractional change in the number of initial oil droplets. The above analysis assumes that the volume fraction is not changed (i.e., $\phi_i = \phi_f \equiv \phi$), and the number of oil droplets decreases from an initial value of N_i to a final value of $N_f = N_i(1-\varepsilon) \equiv N(1-\varepsilon)$. The number of oil droplets in the bulk decreases, and hence, the number of configurations is reduced (i.e., the entropy change is always negative) because oil droplets prefer the formation of surface lenses.

From eqs 16−19, therefore

$$t_N = B_1\phi^{-2/3}\exp\left[\frac{\Delta G_s^{tot}}{k_BT}\right] \exp\left[-\frac{N\varepsilon}{\phi}[\phi \ln \phi + (1-\phi)\ln(1-\phi)] - \frac{\mu N\varepsilon}{k_BT}\right] \tag{20}$$

where B_1 is a constant. Here

$$\Delta G_s^{tot} = \Delta G_s^{nc} + \Delta G_I \tag{21}$$

Equation 20 is a complicated equation which will be tested sequentially by fixing various components in this equation.

When discussing molecular solutions, μ is the chemical potential energy *per molecule*, and all the molecules are the *same* size; there are N molecules present in a system. In eq 17, μ is the chemical potential energy *per 6CB droplet*, and there are N 6CB droplets in a pendant droplet of volume V_p. For a molecular system, μ is a constant as you change N. For our system, μ will be a function of d and therefore a function of N. Here, the chemical potential is calculated using a thermodynamic identity as well as eqs 3 and 19; thus

$$\mu = -T\left(\frac{dS}{dN}\right)_{U,V_p} = -T\left[\left(\frac{\partial S}{\partial N}\right)_{U,V_p,\phi} + \left(\frac{\partial S}{\partial \phi}\right)_{U,V_p,N}\left(\frac{\partial \phi}{\partial N}\right)\right] = -\varepsilon k_BT[\ln \phi - \ln(1-\phi)] \tag{22}$$

Therefore, the nucleation time is expressed as

$$t_N = B_1\phi^{-2/3}\exp\left[\frac{\Delta G_s^{tot}}{k_BT}\right] \exp\left[-\frac{N\varepsilon}{\phi}[\phi \ln \phi + (1-\phi)\ln(1-\phi)] + N\varepsilon^2[\ln \phi - \ln(1-\phi)]\right] \tag{23}$$

At fixed pendant droplet volume V_p, eq 23 is a complex function of N, ϕ, d, and T where N, ϕ, and d are interrelated via eq 3. The numerator ΔG_s^{tot} is expected to depend upon the 6CB droplet diameter d but to be independent of the number N of 6CB droplets; specifically, ΔG_s^{tot} is the free energy change for a *single* 6CB to transform from Figure 1c to Figure 1d. There are N_s 6CB surface droplets, all of diameter d, which are attempting to undergo this surface nucleation transition. N (or equivalently ϕ) determines the number N_s. In order to explore the functional form entailed in eq 23, we systematically vary N, ϕ, d, and T while measuring t_N.

Thus far, the volume fraction ϕ has been varied, at fixed temperature T, for various 6CB droplet diameters d (Figure 3). The temperature dependence of eq 23 is examined next. Figure 5a is a log−linear plot of t_N versus T^{-1} in a temperature range from T = 293 to 299 K at fixed ϕ = 0.000 53 and for various 6CB droplet diameters d, prepared using Method B. (Note: A limited temperature range was studied in order to avoid pendant droplet evaporation effects.) As expected, according to eq 23, the surface nucleation time is well described by an equation of the form

$$t_N = A_1\exp\left[\frac{\Delta G_s^{tot}}{k_BT}\right] \tag{24}$$

https://doi.org/10.1021/acs.langmuir.1c01487
Langmuir 2021, 37, 9588−9596

Table 3. Values for A_1 and ΔG_s^{tot}

d [nm]	N at fixed $\phi = 0.000\,53$[a]	A_1 (s)	ΔG_s^{tot} (J)	A_1^{calc} (s)[b]
403 ± 96	$(2.16 \pm 1.55) \times 10^8$	$(1.12 \pm 0.74) \times 10^{-10}$	$(1.17 \pm 0.03) \times 10^{-19}$	$(1.18 \pm 0.06) \times 10^{-10}$
832 ± 107	$(2.46 \pm 0.95) \times 10^7$	$(1.05 \pm 0.80) \times 10^{-8}$	$(1.00 \pm 0.03) \times 10^{-19}$	$(1.28 \pm 0.14) \times 10^{-8}$
1184 ± 158	$(8.53 \pm 3.42) \times 10^6$	$(4.47 \pm 5.60) \times 10^{-6}$	$(0.78 \pm 0.05) \times 10^{-19}$	$(2.16 \pm 0.10) \times 10^{-6}$
1632 ± 258	$(3.26 \pm 1.55) \times 10^6$	$(2.74 \pm 1.97) \times 10^{-3}$	$(0.63 \pm 0.03) \times 10^{-19}$	

[a] σ_N, the error for N, has been calculated using $\sigma_N = \left|\frac{-18\phi V_p}{\pi d^4}\right| \sigma_d$ from eq 3. [b] The error for A_1^{calc}, $\sigma_{A_1^{calc}}$, is obtained from

$$\sigma_{A_1^{calc}} = \left\{ \begin{array}{l} [\phi^{-2/3} \exp[-C_1(\phi \ln \phi + (1-\phi)\ln(1-\phi))]]^2 \sigma_{B_1}{}^2 + \\ [-(\phi \ln \phi + (1-\phi)\ln(1-\phi))B_1 \phi^{-2/3} \\ \quad \exp[-C_1(\phi \ln \phi + (1-\phi)\ln(1-\phi))]]^2 \sigma_{C_1}{}^2 \end{array} \right\}^{1/2}$$

using eq 31.

Table 4. Equation 26 Best Fit Values

		$\nu = 2/3$							
d [nm]	ΔG_s^{tot} [J]	B_1 [s]	C_1	D_1	ε	B_2 [s]	C_2	D_2	ν
400	11.8×10^{-20}	$(6.83 \pm 0.29) \times 10^{-13}$	26.7 ± 4.3	≈0	$(6.39 \pm 0.27) \times 10^{-11}$	$(5.69 \pm 1.99) \times 10^{-13}$	30.7 ± 12.6	≈0	0.69 ± 0.04
800	9.9×10^{-20}	$(7.32 \pm 0.78) \times 10^{-11}$	30.3 ± 4.4	≈0	$(5.80 \pm 0.62) \times 10^{-10}$	$(8.37 \pm 4.18) \times 10^{-11}$	23.3 ± 15.5	≈0	0.66 ± 0.05
1200	8.1×10^{-20}	$(1.20 \pm 0.05) \times 10^{-8}$	36.3 ± 3.8	≈0	$(2.35 \pm 0.10) \times 10^{-9}$	$(1.39 \pm 0.82) \times 10^{-8}$	33.9 ± 20.6	≈0	0.65 ± 0.06

The solid lines in Figure 5a are fits to eq 24 where the parameters A_1 and ΔG_s^{tot} are listed in Table 3.

In Figure 5b, ΔG_s^{tot} is plotted as a function of d using the data in Table 3. These data are to a good approximation linear with

$$\Delta G_s^{tot} = a + bd \tag{25}$$

where $a = (1.36 \pm 0.04) \times 10^{-19}$ J, and $b = -(4.6 \pm 0.4) \times 10^{-23}$ J/nm. It is not understood at this time why ΔG_s^{tot} decreases with increasing 6CB droplet diameter d.

Since the variation of ΔG_s^{tot} with d has been determined, it is now possible to test other dependencies in eq 23. Equation 23 is rewritten in the following form (with the assistance of eq 3):

$$t_N \phi^\nu = B_i \exp\left[\frac{\Delta G_s^{tot}}{k_B T}\right] \exp[-C_i[\phi \ln \phi + (1-\phi) \ln(1-\phi)] + D_i \phi[\ln \phi - \ln(1-\phi)]] \tag{26}$$

where the amplitudes B_i, C_i, and D_i are adjustable parameters possessing differing meanings depending upon the index i as described below. For index $i = 1$, the exponent ν is fixed at $\nu = 2/3$; the solid lines in Figure 4b represent the best fit to the experimental data for the different droplet diameters $d \approx 400$, 800, and 1200 nm where the values for B_1, C_1, and D_1 are listed in Table 4. In fitting the experimental data to eq 26, the values for ΔG_s^{tot} have been calculated from eq 25 and are given in Table 4. Equation 26 provides a good description of the experimental surface nucleation results, at least for $\phi \lesssim 0.004$ (or equivalently $x \lesssim 10$ mM). Deviations from this behavior, observed at higher ϕ, may be caused by interactions between 6CB droplets in the bulk aqueous phase.

Figure 6 is a log−linear plot of B_1 versus d which demonstrates that

$$B_1 = B_0 \exp[d/d_o] \tag{27}$$

with $d_o = (78.44 \pm 0.05)$ nm and $B_0 = (2.72 \pm 0.03) \times 10^{-15}$ s. In order to understand the dependence of B_1 upon d, exhibited in eq 27, one would need to develop a theory for the nonclassical nucleation process proposed above taking into account any surface charging that may be present.

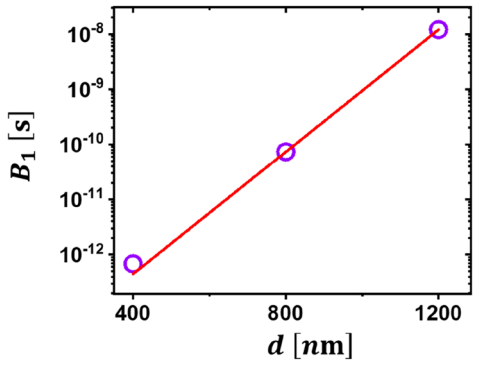

Figure 6. Log−linear plot of B_1 versus d.

From eqs 3 and 26, the parameter

$$\varepsilon = \frac{\pi C_1 d^3}{6 V_p} \tag{28}$$

where the pendant droplet volume is taken as $V_p = 14$ μL. Equation 28 leads to the values for ε given in Table 4. As expected, ε is small where this small value for ε additionally explains why $D_1(\sim\varepsilon^2) \approx 0$ (Table 4) in the fitting process. It would appear, from Table 4, that ε is a sensitive function of d; however, this variation of ε with d is somewhat misleading. Upon comparing eqs 19, 23, and 26, a more important quantity to consider that drives this nonclassical surface nucleation process is the entropy change given by

$$\Delta S = C_1 k_B[\phi \ln \phi + (1-\phi) \ln(1-\phi)] \tag{29}$$

where the experimental results in Table 4 indicate that

$$C_1 (\equiv N\varepsilon/\phi) = 30 \pm 4 \tag{30}$$

A more complete theory would be able to explain the magnitude for C_1.

https://doi.org/10.1021/acs.langmuir.1c01487
Langmuir 2021, 37, 9588−9596

A slightly more general form for eq 26 has also been tested against the experimental data. In this case, for index $i = 2$, there are four adjustable parameters, specifically ν, B_2, C_2, and D_2, where the best fit to the experimental data is shown as the solid lines in Figure 3 while the values for these four parameters are listed in Table 4. This data fitting provides confirmation that $\nu = 2/3$ is an accurate description of the experimental results.

Lastly, the data at constant T (Figure 4 and Table 4) should be self-consistent with data at constant ϕ (Figure 5 and Table 3). Specifically, a comparison of eqs 24 and 26 would imply the following interconnection between these data sets

$$A_1 = B_1\phi^{-2/3}\exp[-C_1(\phi \ln \phi + (1-\phi)\ln(1-\phi))] \quad (31)$$

A_1^{calc}, in Table 3, is deduced from eq 31 with $\phi = 0.000\,53$ where B_1 and C_1 are obtained from Table 4. A_1^{calc} qualitatively agrees with the A_1 fitting parameter in Table 3 where the differences may arise from the linear averaging for ΔG_s^{tot} in Figure 5b.

5. CONCLUSION

In this publication, a new type of surface nucleation process, which occurs in nanoemulsion systems, is studied. In the initial state, nanoemulsion droplets of oil are dispersed throughout a bulk aqueous phase where the emulsion−air surface resides in a *metastable surface state* possessing a surface energy characteristic of pure water ($\gamma \sim 72$ mN/m). Nano-oil droplets, in the vicinity of the surface, therefore possess an effective contact angle of $\theta = 180°$. In the final equilibrium state, the emulsion−air surface is covered by a 6CB layer of lower surface energy $\gamma \sim 66$ mN/m (Figure 2b) at pseudopartial wetting with spreading coefficient $S > 0$ and Hamaker constant $W < 0$. [A 6CB droplet placed at such an air−dispersion surface possesses a finite contact angle ($\alpha + \beta = 0.22°$, Figure 2a, lower inset) and is in equilibrium with this 6CB surface layer.] The transition from the initial metastable surface state to the final equilibrium surface state is thought to arise via a nonclassical surface nucleation process where a near surface 6CB nanodroplet (Figure 1c) is transformed into a surface nanolens (Figure 1d). For this morphological transformation to occur, a surface 6CB nanodroplet must overcome an energy barrier. "Tunneling" through this energy barrier takes time, the surface nucleation time t_N. This tunneling event is characterized by an abrupt decrease in the surface tension at t_N (Figure 2b). The nucleation time data t_N, which are available in the Supporting Information, are found to depend sensitively upon the bulk 6CB volume fraction ϕ and 6CB droplet diameter d (Figure 3), as well as the temperature T (Figure 5a).

A consideration of the number of 6CB nanodroplets in the vicinity of the air−dispersion surface as well as the bulk entropy change associated with the nucleation process gives rise to a model, eq 26 together with eq 3, which explains this dependence of t_N upon ϕ, d, and T, at least at low $\phi < 0.004$. Our model assumes that 6CB nanodroplets *in the bulk* act as an ideal gas where interactions between 6CB nanodroplets can be ignored. Deviations from this model, found at higher ϕ (>0.004), may arise from departures from this ideal gas assumption. Our model is incomplete as the model contains a number of adjustable parameters: ΔG_s^{tot}, B_1, and C_1. A more complete theory would provide an explanation for the dependence of ΔG_s^{tot} (Figure 5b, eq 25) and B_1 (Figure 6, eq 27) upon d, as well as the value for C_1 (eq 30). In developing a theory for ΔG_s^{tot}, B_1, and C_1, as the air−water and oil−water surfaces are negatively charged (and screened by counterions), one would need to consider the electrical double layer repulsion between a negatively charged 6CB droplet and the negatively charged air−water surface, an attractive van der Waals interaction, as well as any electrohydrodynamic processes that would play a role in converting a near surface spherical 6CB droplet (Figure 1c) into a 6CB nanolens (Figure 1d) at the air−water surface. This problem has similarities to DLVO theory[14] except that one is now examining the coalescence of a charged oil droplet in the aqueous phase with a charged air−water surface. To be consistent with other work and to be as realistic as possible one should combine the Lippmann equation[22] with the Neumann−Young equations (eqs 1a and 1b) where, in addition, the isoelectric points[7,23] for both the air−water and oil−water surfaces are considered within the Poisson−Boltzmann equation. As far as we are aware, the coalescence of a nano-oil droplet with the air−water surface from a nanoemulsion has never been considered as an initiator of surface nucleation. Instead, prior experimental[15,16,24,25] and theoretical[26−32] studies have primarily dealt with wetting transitions in oil−water systems[15,24] and how wetting transitions are influence by the presence of salt[16,25−27,31] or how salt in aqueous solutions influences the interfacial tension,[28] bulk phase diagram,[29,30] or surface phase diagram.[32]

■ ASSOCIATED CONTENT

Supporting Information

The Supporting Information is available free of charge at https://pubs.acs.org/doi/10.1021/acs.langmuir.1c01487.

Nucleation time t_N at constant temperature $T = 295$ K for various 6CB volume fractions ϕ and nanodroplet diameters d; and t_N at constant $\phi = 0.000\,53$ for various T and d (PDF)

■ AUTHOR INFORMATION

Corresponding Authors

Bruce M. Law − *Department of Physics, Kansas State University, Manhattan, Kansas 66506, United States;* orcid.org/0000-0002-3877-8497; Email: bmlaw@phys.ksu.edu

Hyuk Kyu Pak − *Center for Soft and Living Matter, Institute for Basic Science (IBS), Ulsan 44919, Republic of Korea; Department of Physics, Ulsan National Institute of Science and Technology (UNIST), Ulsan 44919, Republic of Korea;* Email: hyuk.k.pak@gmail.com

Authors

Jin Tae Park − *Center for Soft and Living Matter, Institute for Basic Science (IBS), Ulsan 44919, Republic of Korea; Department of Physics, Ulsan National Institute of Science and Technology (UNIST), Ulsan 44919, Republic of Korea*

Govind Paneru − *Center for Soft and Living Matter, Institute for Basic Science (IBS), Ulsan 44919, Republic of Korea; Department of Physics, Ulsan National Institute of Science and Technology (UNIST), Ulsan 44919, Republic of Korea*

Masao Iwamatsu − *Department of Physics, Tokyo Metropolitan University, Hachioji, Tokyo 192-0397, Japan; Department of Physics, Tokyo City University, Setagaya-ku, Tokyo 158-8557, Japan*

Complete contact information is available at: https://pubs.acs.org/10.1021/acs.langmuir.1c01487

Notes

The authors declare no competing financial interest.

■ ACKNOWLEDGMENTS

The authors thank Mr. K. Chiguchi (Kyushu University) and Professor H. Matsubara (Hiroshima University) for discussions and comments. B.M.L. wishes to thank the IBS Center for Soft and Living Matter at UNIST for their kind hospitality and support during his stays at UNIST. This work was supported by the American Chemical Society Petroleum Research Fund grant PRF 58043-ND5 (B.M.L.) and the Korean government with grant IBS-R020-D1 (H.K.P.).

■ REFERENCES

(1) Law, B. M. Theory of nucleated wetting. *Phys. Rev. Lett.* **1994**, *72*, 1698−1701.
(2) Law, B. M.; Pak, H. K. Influence of hydrodynamic flow on nucleated wetting. *J. Chem. Phys.* **1997**, *106*, 301−310.
(3) Herminghaus, S.; Jacobs, K.; Mecke, K.; Bischof, J.; Fery, A.; Ibn-Elhaj, M.; Schlagowski, S. Spinodal dewetting in liquid crystal and liquid metal films. *Science* **1998**, *282* (5390), 916.
(4) Campbell, J. M.; Christenson, H. K. Nucleation- and emergence-limited growth of ice from pores. *Phys. Rev. Lett.* **2018**, *120*, 165701.
(5) Aveyard, R.; Clint, J. H.; Nees, D.; Paunov, V. Size-dependent lens angles for small oil lenses on water. *Colloids Surf., A* **1999**, *146*, 95−111.
(6) *ChemicalBook: CAS DataBase List.* www.chemicalbook.com/ChemicalProductProperty_EN_CB7311970.htm.
(7) Creux, P.; Lachaise, J.; Graciaa, A.; Beattie, J. K.; Djerdjev, A. M. Strong specific hydroxide ion binding at the pristine oil/water and air/water interfaces. *J. Phys. Chem. B* **2009**, *113*, 14146−14150.
(8) Adamson, A. W. *Physical chemistry of surfaces*, 4th ed.; Wiley: New York, 1982.
(9) Tintaru, M.; Moldovan, R.; Beica, T.; Frunza, S. Surface tension of some liquid crystals in the cyanobiphenyl series. *Liq. Cryst.* **2001**, *28* (5), 793−797.
(10) De Gennes, P. G. Wetting: Statics and dynamics. *Rev. Mod. Phys.* **1985**, *57*, 827−863.
(11) Law, B. M. Wetting, adsorption and surface critical phenomena. *Prog. Surf. Sci.* **2001**, *66*, 159−216.
(12) de Gennes, P.-G.; Brochard-Wyart, F.; Quere, D. *Capillarity and wetting phenomena*; Springer: New York, 2004.
(13) Bonn, D.; Eggers, J.; Indekeu, J.; Meunier, J.; Rolley, E. Wetting and spreading. *Rev. Mod. Phys.* **2009**, *81*, 739−805.
(14) Israelachvili, J. N. *Intermolecular and surface forces*, 3rd ed.; Academic Press: London, UK, 2011.
(15) Ragil, K.; Meunier, J.; Broseta, D.; Indekeu, J. O.; Bonn, D. Experimental observation of critical wetting. *Phys. Rev. Lett.* **1996**, *77*, 1532−1535.
(16) Shahidzadeh, N.; Bonn, D.; Ragil, K.; Broseta, D.; Meunier, J. Sequence of two wetting transitions induced by tuning the Hamaker constant. *Phys. Rev. Lett.* **1998**, *80*, 3992−3995.
(17) *CRC handbook of chemistry and physics*, 66th ed.; CRC Press, Inc.: Boca Raton, 1985.
(18) Li, J.; Gauzia, S.; Wu, S.-T. High temperature-gradient refractive index liquid crystals. *Opt. Express* **2004**, *12* (9), 2002−2010.
(19) Ratna, B. R.; Shashidhar, R. Dielectric properties of 4'-n-alkyl-4-cyanobiphenyls in their nematic phases. *Pramana* **1976**, *6* (5), 278−283.
(20) Hunter, R. J. *Foundations of colloid science*; Oxford University Press: Oxford, 2001.
(21) McClements, D. J. Nanoemulsions versus microemulsions: terminology, differences. *Soft Matter* **2012**, *8* (6), 1719−1729.
(22) Mugele, F.; Baret, J.-C. Electrowetting: from basics to applications. *J. Phys.: Condens. Matter* **2005**, *17*, R705−R774.
(23) Larson, I.; Attard, P. Surface charge of silver iodide and several metal oxides. Are all surfaces Nernstian? *J. Colloid Interface Sci.* **2000**, *227*, 152−163.
(24) Pohl, D. W.; Goldburg, W. I. Wetting transition in Lutidine-water mixtures. *Phys. Rev. Lett.* **1982**, *48*, 1111−1114.
(25) Sigl, L.; Fenzl, W. Order-parameter exponent β_1 of a binary liquid mixture at a bouondary. *Phys. Rev. Lett.* **1986**, *57*, 2191−2194.
(26) Weiss, V. C.; Indekeu, J. O. Effect of ion hydration on the first-order transition in the sequential wetting of hexane on brine. *J. Chem. Phys.* **2003**, *118* (23), 10741−10751.
(27) Denesyuk, N. A.; Hansen, J.-P. Wetting transitions of ionic solutions. *J. Chem. Phys.* **2004**, *121*, 3613−3624.
(28) Onuki, A. Surface tension of electrolytes: hydrophilic and hydrophobic ions near an interface. *J. Chem. Phys.* **2008**, *128*, 224704.
(29) Onuki, A.; Okamoto, R. Selective solvation effects in phase separation in aqueous mixtures. *Curr. Opin. Colloid Interface Sci.* **2011**, *16*, 525−533.
(30) Okamoto, R.; Onuki, A. Charged colloids in an aqueous mixture with a salt. *Phys. Rev. E* **2011**, *84*, No. 051401.
(31) Ibagon, I.; Bier, M.; Dietrich, S. Order of wetting transitions in electrolyte solutions. *J. Chem. Phys.* **2014**, *140*, 174713.
(32) Yabunaka, S.; Onuki, A. Electric double layer composed of an antagonistic salt in an aqueous mixture: local charge separation and surface phase transition. *Phys. Rev. Lett.* **2017**, *119*, 118001.

https://doi.org/10.1021/acs.langmuir.1c01487
Langmuir 2021, 37, 9588−9596